XMM-Newton observation of the X-ray point source population of the starburst galaxy IC 342

Albert K. H. Kong[*]

Harvard-Smithsonian Center for Astrophysics, 60 Garden Street, Cambridge, MA 02138, USA

ABSTRACT

We present the results of an *XMM-Newton* observation of the starburst galaxy IC 342. Thirty-seven X-ray point sources were detected down to a luminosity limit of $\sim 10^{37}$ $\mathrm{erg\,s^{-1}}$. Most of the sources are located near the spiral arms. The X-ray point source luminosity function is consistent with a power-law shape with a slope of 0.55, typical of starburst galaxies. We also present the energy spectra of several ultraluminous X-ray sources (ULXs), including the luminous X-ray source in the galactic nucleus. Except for the nucleus and a luminous supersoft X-ray source, other ULXs can generally be fit with a simple power-law spectral model. The nucleus is very luminous ($\sim 10^{40}\,\mathrm{erg\,s^{-1}}$ in 0.2–12 keV) and requires disc blackbody and power-law components to describe the X-ray emission. The spectral fit reveals a cool accretion disc ($kT = 0.11$ keV) and suggests that the source harbours either an intermediate-mass black hole or a stellar-mass black hole with outflow.

Key words: galaxies: individual: IC 342 – X-rays: binaries – X-rays: galaxies.

1 INTRODUCTION

IC 342 is a nearby late-type Sc galaxy in the Maffei Group which is one of the closest groups to our Galaxy. The spiral arms of IC 342 is well developed and is almost face-on ($i = 25° \pm 3°$; Newton 1980). IC 342 also shows substantial nuclear star formation (Becklin et al. 1980; Rickard & Harvey 1984). IC 342 has been observed with *Einstein* (Fabbiano & Trinchieri 1987), *ROSAT* (Bregman, Cox, & Tomisakam 1993) and *ASCA* (Okada et al. 1998; Kubota et al. 2001) previously. Ten X-ray point sources were found in the *ROSAT* HRI observation. IC 342 is also well known to house several ultraluminous X-ray sources (ULXs; Roberts & Warwick 2000). In particular, X1 and X2 (based on designations in Okada et al. 1998) showed spectral and intensity transition during the *ASCA* observations taken in 1993 and 2000 (Kubota et al. 2001). The state transitions of the two ULXs resemble the spectral/intensity states of X-ray transients in our Galaxy. In addition, a periodicity of 31 hr or 41 hr was found in X-2 with long (~ 250ks net exposure time) *ASCA* observations (Sugiho et al. 2001). Although we have known that there are several point sources around the galaxy nucleus based on *ROSAT* HRI data, the angular resolution of *ASCA* is very low and the nucleus of IC 342 is not resolved. Hence, we know very little about the X-ray emission from the nucleus. With the advent of *XMM-Newton*, we now have

sufficient resolving power and collective area to have a detailed study of the galaxy.

At a distance of 1.8 Mpc (see Buta and McCall 1999 for a review), $1''$ corresponds to 8.7 pc. Its proximity and its almost face-on orientation towards the observer provides a unique possibility to study the X-ray point source populations. Unfortunately, IC 342 is located at low Galactic latitude ($b = 10°.6$), resulting a relatively high hydrogen column density, $N_H = 3 \times 10^{21}$ cm^{-2} (Dickey & Lockman 1990). This limits us to constrain local absorption and X-ray emission below 1 keV.

In this paper, we report on the X-ray point sources detected in IC 342, with an archival *XMM-Newton* observation. We begin with a description of the observation and data reduction procedures. In Section 3, we present the results of our study including the global properties of X-ray sources, spectral fits to bright sources, and the X-ray luminosity function. In Section 4, we discuss the X-ray source population, the nucleus and the ULXs of this galaxy. A summary will be given in Section 5.

2 OBSERVATIONS AND DATA REDUCTION

IC 342 was observed with the three instruments of European Photon Imaging Camera (EPIC) and the Optical Monitor (OM) on board *XMM-Newton* on 2001 February 11 for about 10ks. The instrument modes were full-frame with medium optical blocking filter for the pn and the two MOS cam-

eras, while the filter of OM was $UVW1$ (bandpass between 2200Å and 4000Å). The event files were reprocessed and filtered with the *XMM-Newton* Science Analysis Software (SAS v5.4.1). Only data in 0.2-12 keV were used for analysis. We constructed light curves of source-free regions from each of the three instruments and after rejecting intervals with a high background level, we obtained a good time interval of 5ks and 9.5ks for the pn and MOS cameras, respectively.

We created a combined MOS image by merging the two MOS detectors (MOS-1 and MOS-2) to increase the signal-to-noise (S/N) level. We also obtained a merged image from the three detectors. Figure 1 shows the merged EPIC image of the central $20' \times 20'$ region of IC 342. Source detection was done on the pn, merged MOS, and pn+MOS images with SAS task EWAVELET, with a detection threshold of 5σ. We examined the existence and position of each detected source by checking individual and merged images. The OM image and source detection were performed with the standard SAS pipeline tasks. We also corrected the astrometry of the OM image by using the USNO catalogue (Monet et al. 1998). The OM image of the central $8' \times 8'$ region of IC 342 is shown in Figure 2.

Source count rates were determined via aperture photometry with source-free regions as the background and were corrected for effective exposure and vignetting. The radius of the aperture was varied with average off-axis angle in order to match the 90% encircled energy function. The count rates reported here are the pn count rates in the total (0.2-12 keV), soft (0.2-1 keV), medium (1-2 keV), and high (2-12 keV) bands. Some sources fell in the chip boundary or outside the field of view of the pn camera. We then used the MOS count rates and rescaled them to the pn values with PIMMS. Energy spectra of bright sources were extracted with the SAS task XMMSELECT. Source-free regions were used for background. Response matrices were created by RMFGEN and ARFGEN.

3 RESULTS

3.1 Properties of X-ray sources

We detected 37 X-ray point sources in IC 342 (Table 1). The sources are mainly concentrated in the spiral arms of the galaxy (see Fig. 3). Five of the detected sources were clearly associated with bright stellar object within $5''$ in the Digitized Sky Survey (DSS; Fig. 3) and the OM (Fig. 2) images. Source 12 (X12 hereafter) was also previously associated with a star in the *ROSAT* observation (Source 4 in Bregman et al. 1993). We then used the 3 matches within the central $5'$ region to correct the astrometry of the X-ray images with the USNO catalogue. The positions listed in Table 1 and throughout this paper use this astrometric reference. The conversion of luminosities assumes an absorbed power-law spectrum with a photon index of 2 and $N_H = 8 \times 10^{21}$ cm^{-2} (the average from the spectral fits; see § 3.2). The detection limit is $\sim 1.3 \times 10^{37}$ erg s^{-1} in the 0.2–12 keV band. Of the 37 sources, 9 of them were detected in previous *ROSAT* HRI observation (Bregman et al. 1993). One *ROSAT* source (source 2 in Bregman et al. 1993) is below the *XMM-Newton* detection limit, which suggests that the source is fainter by a factor of ~ 7 between the two observations.
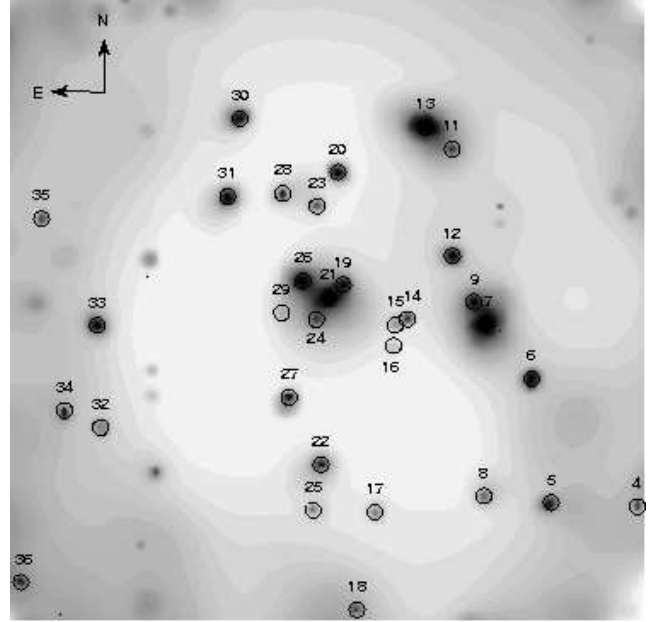

Figure 1. Merged EPIC (pn + MOS-1 + MOS-2) image (0.2-12 keV) of the central $20' \times 20'$ region of IC 342. The image has been exposure corrected and adaptively smoothed. The circles have a radius of $15''$. Some apparent "sources" (which are not included in the source list) in the image are artifacts of the detector.
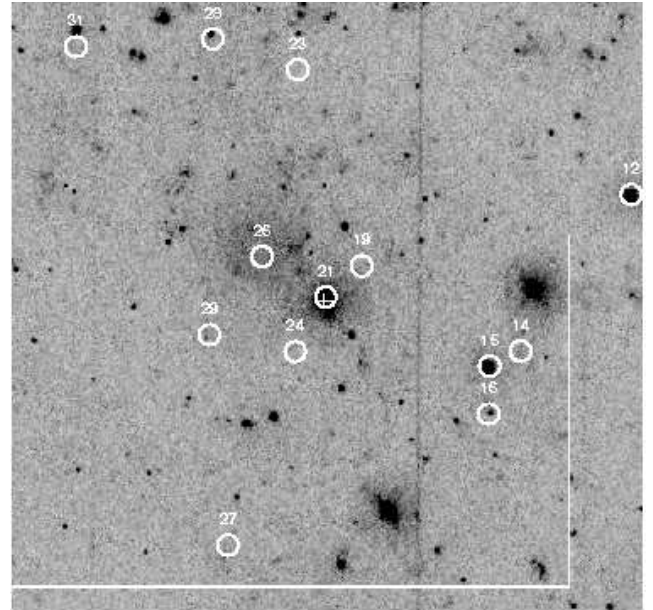

Figure 2. Optical Monitor (OM) image of the central $8' \times 8'$ region of IC 342 in the $UVW1$ filter. The circles (radius of $8''$) correspond to the X-ray sources identified from the *XMM-Newton* images. The dynamical centre of the galaxy (Turner et al. 1992) is marked with a cross which is coincident with X21.

Many of the detected sources have < 100 counts, which makes it difficult to derive spectral parameters. However, hardness ratios can give a crude indication of the X-ray spectra. Following Kong et al. (2002), we computed the hardness ratios for each detected sources, which are defined as HR1=(medium-soft)/(medium+soft) and HR2=(hard-
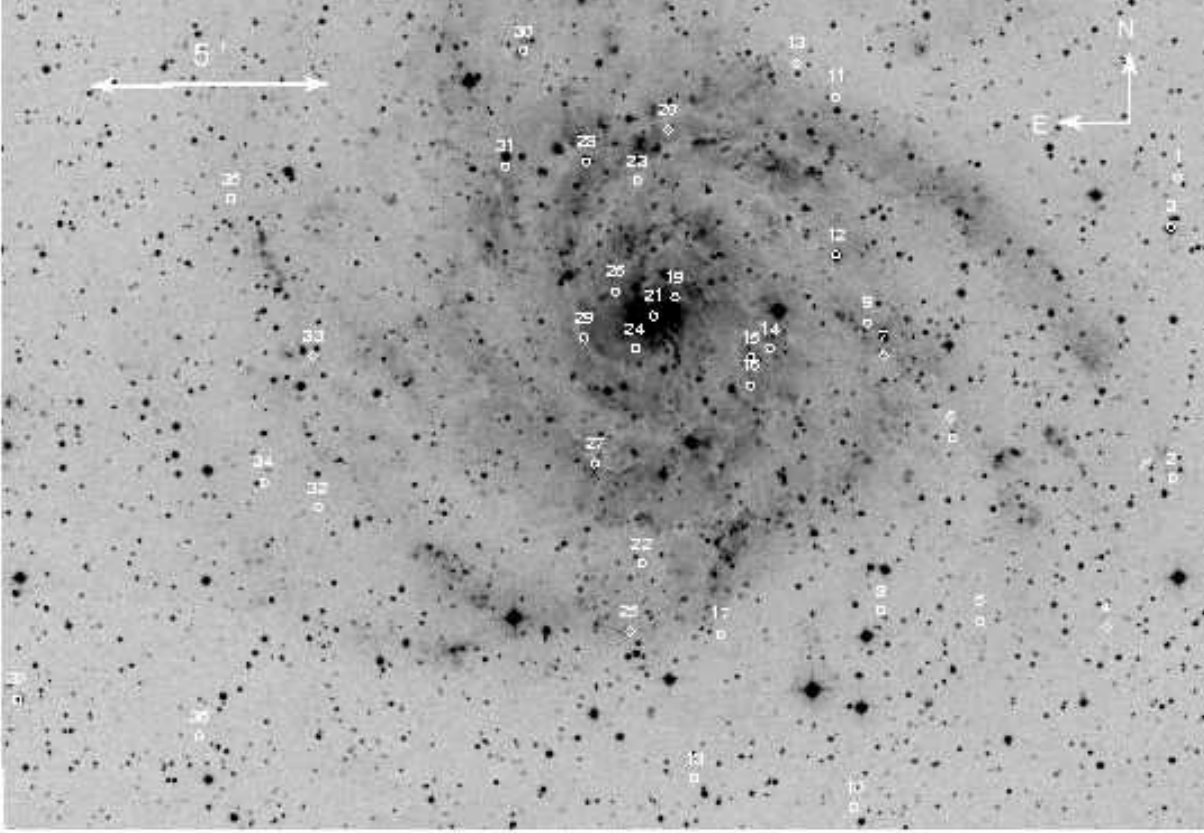
Figure 3. Digitized Sky Survey (DSS) blue band image of IC 342, with detected *XMM-Newton* X-ray sources overplotted (see Table 1 for the source list). The circles have a radius of $5''$.

soft)/(hard+soft). Figure 4 shows the colour-colour diagram for all detected sources. We have overlaid the colour-colour diagram with lines showing the tracks followed by representative spectral models with differing values of N_H. We have shown in the diagram for power-law models with photon index ranges from 1.2 to 3, a Raymond-Smith thermal model with $kT_{RS} = 0.5$ keV, and a blackbody model with $kT = 0.1$ keV. For each model, the N_H increases from the left to the right, from $N_H = 3 \times 10^{21}$ cm^{-2} to $N_H = 10^{22}$ cm^{-2}. Power-law spectra tend to occupy the top right section of the diagram, while soft thermal models occupy the lower left.

It is clear that many of the sources are consistent with a power-law spectral model, while a few of them are dominated by soft X-ray emission. These soft X-ray sources are likely to be supersoft sources (Di Stefano & Kong 2003), supernova remnants or foreground stars. For example, foreground star X12 has HR1=−0.58 and HR2=−0.90.

The closest X-ray source to the dynamical galaxy centre (Turner et al. 1992; marked with a white cross in Figure 2), X21, is about $3''$ (26.1 pc) from the galactic centre and is within the positional accuracy of *XMM-Newton*. It it worth noting that X21 is also seen in the *ROSAT* HRI image, but in the *Einstein* and *ASCA* images, X21 is not resolved from several nearby sources (see Figure 1). The galaxy centre was also detected as a point-like UV source in the OM, with $UVW1 = 13.6$.

3.2 Spectral fits of bright sources

We extracted the energy spectra for sources that have > 100 counts, and fitted them to simple one-component spectral models including absorbed power-law, blackbody, disc blackbody, Raymond-Smith, broken powerlaw and the bulk motion Comptonization (BMC; Shrader & Titarchuk 1999) models. Except for X12, X20, and X21, all sources were satisfactorily fitted with simple absorbed power-law model (see Table 2). Generally, the N_H of the brightest sources ranges from 3×10^{21}cm^{-2} to 2×10^{22}cm^{-2} with an average of 8×10^{21} cm^{-2}, while the photon index varies between 1.7 and 3.2. These spectra are consistent with typical X-ray binaries seen in our Galaxy and other external galaxies. For X7 and X13, the spectra can be fitted equally well with a disc blackbody model with inner disc temperature of ~ 2 keV. Figure 5 shows the disc blackbody spectrum of X7. Both X7 and X13 are two of the previously reported ULXs in IC 342 and our results are in good agreement with previous *ASCA* observations (see § 4.3 for discussion). For X12 and X20, their spectra are soft and can be fit with a blackbody model. X12 is likely to be a foreground star and the soft spectrum is not unexpected. The blackbody temperature of X20 is ~ 0.1 keV, suggesting that it is a luminous supersoft X-ray sources (Di Stefano & Kong 2003). It is worth noting that X20 was also detected by *ROSAT* HRI (Bregman et al. 1993). If we assumed the same spectral shape as the *XMM-Newton* observation, X20 is about a factor 2 brighter during the *ROSAT* observations.

Table 1. *XMM-Newton* source list of IC 342

ID	R.A. (J2000.0)	Dec. (J2000.0)	Net Counts 0.2–1 keV	Net Counts 1–2 keV	Net Counts 2–12 keV	$L_X{}^a$ ($\times 10^{38}$)	Note
X1	03:44:47.5	+68:08:45.6	52.0 ± 10.1	290.4 ± 18.9	218.6 ± 18.0	1.11	
X2	03:44:49.4	+68:02:17.5	0.0 ± 4.9	108.7 ± 12.0	167.4 ± 16.0	0.53	
X3	03:44:49.3	+68:07:42.1	38.9 ± 10.8	59.4 ± 9.9	-2.7 ± 4.4	0.25	$B = 13.1,\ R = 12.3$
X4	03:45:04.6	+67:59:05.6	-2.682 ± 3.3	11.1 ± 4.6	9.1 ± 6.6	0.14	
X5	03:45:33.6	+67:59:14.4	6.7 ± 6.4	222.6 ± 16.8	1.7 ± 6.2	0.84	
X6	03:45:39.9	+68:03:11.6	58.1 ± 23.6	327.7 ± 18.9	113.8 ± 11.8	1.64	*ROSAT*#1
X7	03:45:55.4	+68:04:57.6	194.0 ± 14.4	885.0 ± 29.9	1079.6 ± 33.2	16.74	*ROSAT*#3
X8	03:45:56.4	+67:59:28.2	3.8 ± 3.8	8.0 ± 3.9	17.6 ± 6.1	0.23	
X9	03:45:59.2	+68:05:39.9	18.5 ± 5.1	69.3 ± 8.6	96.8 ± 10.4	1.43	
X10	03:46:02.6	+67:55:14.2	11.2 ± 5.7	7.2 ± 3.8	11.4 ± 6.5	0.21	
X11	03:46:06.3	+68:10:32.3	3.5 ± 4.1	13.8 ± 4.6	33.9 ± 7.5	0.40	
X12	03:46:06.5	+68:07:07.8	117.2 ± 11.4	31.5 ± 6.1	5.9 ± 4.7	1.20	$B = 12.4,\ R = 12.5,$ *ROSAT*#4
X13	03:46:15.4	+68:11:15.6	14.7 ± 5.0	320.3 ± 18.0	1178.4 ± 34.6	11.79	*ROSAT*#5
X14	03:46:21.8	+68:05:07.7	0.0 ± 1.3	115.5 ± 11.1	3.1 ± 2.8	0.34	
X15	03:46:26.0	+68:04:56.2	16.9 ± 4.5	16.8 ± 4.3	1.9 ± 2.6	0.26	$B = 13.5,\ R = 14.1$
X16	03:46:26.2	+68:04:19.4	10.6 ± 4.0	13.9 ± 4.1	4.4 ± 3.9	0.23	$B = 16.7,\ R = 16.6$
X17	03:46:33.1	+67:58:57.9	1.9 ± 3.8	11.6 ± 4.3	10.7 ± 6.0	0.19	
X18	03:46:39.2	+67:55:51.9	-5.6 ± 2.0	-6.4 ± 1.2	31.3 ± 8.0	0.15	
X19	03:46:43.5	+68:06:13.6	22.4 ± 5.1	71.0 ± 8.5	76.6 ± 9.1	1.32	*ROSAT*#6
X20	03:46:45.1	+68:09:49.7	98.1 ± 10.3	12.8 ± 4.4	4.8 ± 5.1	0.90	*ROSAT*#7
X21	03:46:48.4	+68:05:49.6	316.3 ± 17.9	369.5 ± 20.0	181.5 ± 13.8	6.74	nucleus, *ROSAT*#8
X22	03:46:51.2	+68:00:30.0	-1.3 ± 3.4	27.2 ± 5.8	29.0 ± 6.8	0.43	
X23	03:46:52.2	+68:08:44.8	-2.7 ± 2.9	17.2 ± 5.0	16.2 ± 5.4	0.24	
X24	03:46:52.7	+68:05:07.7	22.6 ± 5.3	22.7 ± 5.0	19.5 ± 5.3	0.51	
X25	03:46:53.8	+67:59:02.3	18.5 ± 5.6	12.1 ± 4.0	2.3 ± 4.7	0.26	
X26	03:46:57.2	+68:06:21.1	197.7 ± 16.8	1083.3 ± 33.1	204.2 ± 14.7	4.56	*ROSAT*#9
X27	03:47:01.9	+68:02:38.6	16.4 ± 5.4	22.2 ± 5.4	21.1 ± 6.2	0.45	
X28	03:47:03.9	+68:09:08.7	9.0 ± 4.7	19.2 ± 4.9	25.2 ± 6.6	0.42	
X29	03:47:04.4	+68:05:20.8	14.2 ± 4.9	12.7 ± 4.1	1.9 ± 4.4	0.23	
X30	03:47:18.4	+68:11:31.9	41.2 ± 7.3	72.1 ± 9.0	29.3 ± 7.1	1.12	
X31	03:47:22.7	+68:09:02.6	28.1 ± 6.5	69.2 ± 8.9	34.6 ± 7.4	1.02	
X32	03:48:05.6	+68:01:41.0	45.4 ± 8.7	50.1 ± 9.7	-6.2 ± 4.3	0.20	
X33	03:48:06.8	+68:04:56.1	31.3 ± 6.5	69.8 ± 8.7	43.4 ± 7.9	1.13	*ROSAT*#10
X34	03:48:17.9	+68:02:13.2	0.5 ± 3.7	22.6 ± 5.2	17.2 ± 6.6	0.30	
X35	03:48:25.9	+68:08:19.6	-0.4 ± 3.9	9.0 ± 4.2	15.5 ± 6.0	0.19	
X36	03:48:32.3	+67:56:43.9	8.4 ± 6.4	70.3 ± 11.9	10.9 ± 7.0	0.36	
X37	03:49:14.0	+67:57:30.0	8.1 ± 4.2	42.8 ± 7.1	43.0 ± 8.3	0.74	$B = 14.0,\ R = 13.0$

X-ray sources associated with stars are indicated by the B and R magnitudes taken from the USNO catalogue. Sources detected by *ROSAT* HRI (Bregman et al. 1993) are noted.
^{a} Unabsorbed 0.2–12 keV luminosity in unit of $\mathrm{erg\,s^{-1}}$, by assuming a power-law spectrum with $N_H = 8 \times 10^{21}\ \mathrm{cm^{-2}}$ and $\alpha = 2$.

X21 is about $3''$ from the dynamical centre and probably is the nucleus of the galaxy (see §4.2 for discussion). Single-component spectral models cannot give a good fit (see Table 2) and it requires a more complicated model. We fit X21 with a two-component model consisting of disc blackbody and power-law components. The additional component significantly ($> 99.9\%$ confidence) improves the fit. We also considered the BMC model and the spectral fit is comparable to the disc blackbody + power-law model. The blackbody temperatures of both models are similar and are low ($kT \approx 0.1$ keV) compared with many ULXs. Depending on the spectral model, the 0.2–12 keV luminosity is between $6 \times 10^{39}\ \mathrm{erg\,s^{-1}}$ and $1.6 \times 10^{40}\ \mathrm{erg\,s^{-1}}$. The best-fitting disc blackbody + power-law model is shown in Figure 6.

3.3   X-ray luminosity function

We constructed the X-ray point source luminosity function to investigate the compact object populations of IC 342 (Wu

2001; Kilgard et al. 2002). The count rates for all detected sources were converted into unabsorbed 0.2–12 keV luminosities by assuming an absorbed power-law model with $N_H = 8 \times 10^{21}\ \mathrm{cm^{-2}}$ and $\alpha = 2$. For the brightest 12 sources (Table 2), we used the luminosities derived from the best-fitting spectral model. In addition, we excluded the three foreground stars (X3, X12, X15, X16 and X37). In Figure 7, we plot the cumulative luminosity function for all sources (excluding the foreground stars). To estimate the completeness limit, we used a method described by Kong et al. (2002). We computed histogram of the number of detected sources against the S/N to examine the completeness limit; the histogram peaks at S/N ~ 5, corresponding to $\sim 3 \times 10^{37}\ \mathrm{erg\,s^{-1}}$, and fall off below this. Hence the luminosity function is complete down to $\sim 3 \times 10^{37}\ \mathrm{erg\,s^{-1}}$. We fit the luminosity function with a simple power-law model and determined the slope via maximum likelihood method on the differential luminosity function ($dN/dL \propto L^{-\beta}$; e.g., Crawford, Jauncey, & Murdoch 1970). We note that the ex-
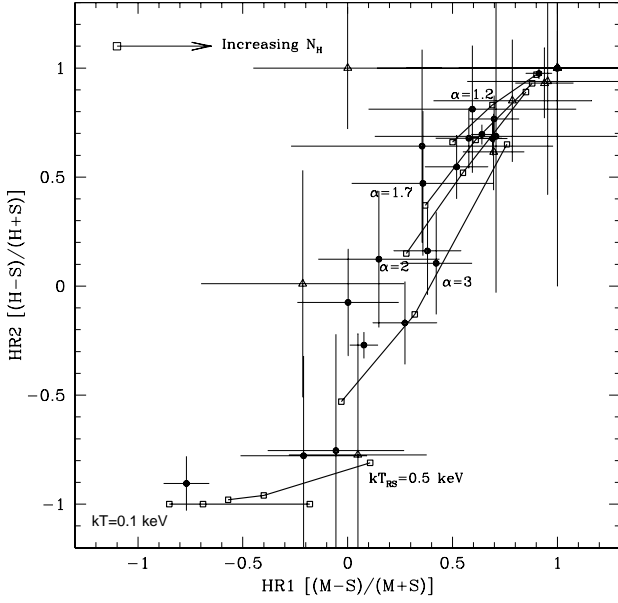
Figure 4. Colour-colour diagram for all detected sources excluding the foreground stars (circles: sources within the D_{25} ellipse; triangles: sources outside the D_{25} ellipse). Also plotted are the hardness ratios estimated from different spectral models. Top to bottom: Power-law model with α of 1.2, 1.7, 2, and 3, Raymond-Smith model with kT_{RS} of 0.5 keV, and blackbody model with kT of 0.1 keV. For each model, N_H varies from the left from $3 \times 10^{21} cm^{-2}$, $5 \times 10^{21} cm^{-2}$, and $10^{22} cm^{-2}$.
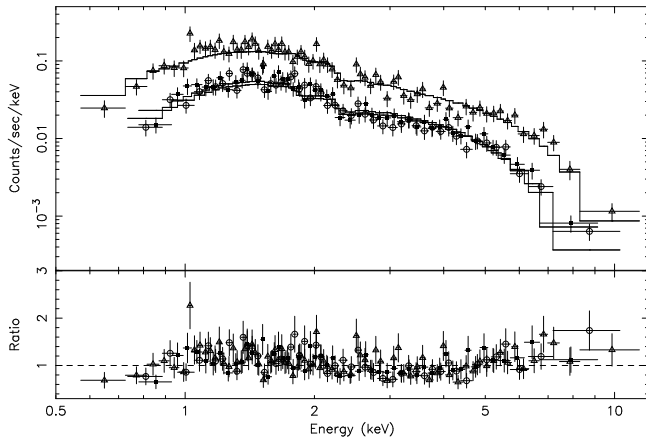

Figure 5. Energy spectrum of X7 (IC 342 X-1 in Okada et al. 1998). pn, MOS-1, and MOS-2 data are marked as triangles, solid squares and circles, respectively. The spectrum can be fitted with a disc blackbody model with $N_H = 3.2 \times 10^{21}$ cm^{-2} and $kT_{in} = 1.98$ keV.

ponent for a fit to cumulative function would be $\Gamma = \beta - 1$. We obtained a slope of 0.55 ± 0.07 for the cumulative luminosity function, with luminosities greater than 10^{37} erg s^{-1}. There are 12 sources outside the D_{25} disc of IC 342 and they are likely to be contaminated by foreground or background objects. Excluding point sources outside the D_{25} ellipse, the slope ($\Gamma = 0.51 \pm 0.07$) is in good agreement with the above result. Within the D_{25} ellipse, we estimated that there are
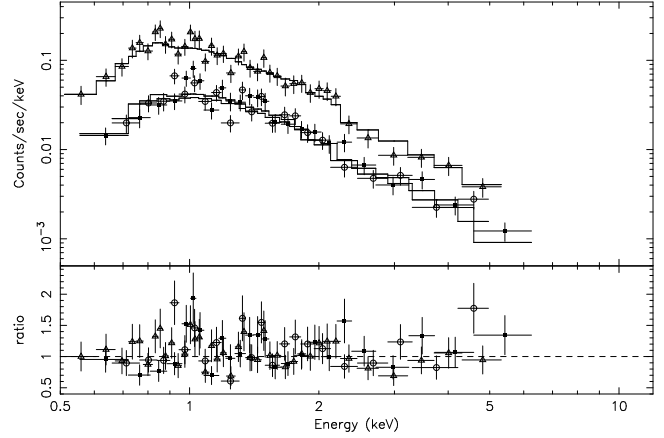
Figure 6. Energy spectrum of the nuclear source (X21). pn, MOS-1, and MOS-2 data are marked as triangles, solid squares and circles, respectively. The spectrum can be fitted with a disc blacbody + power-law model with $N_H = 8.7 \times 10^{21}$ cm^{-2}, $\alpha = 2.73$, and $kT_{in} = 0.11$ keV.

Table 2. Spectral fits to the brightest X-ray sources in IC 342

ID	N_H $(10^{22}cm^{-2})$	α	kT (keV)	χ^2_ν/dof	$L_X{}^a$
X6	$1.32^{+0.90}_{-0.71}$	$2.53^{+1.03}_{-0.73}$		0.4/7	2.23
X7	$0.60^{+0.06}_{-0.05}$	$1.72^{+0.08}_{-0.08}$		0.81/174	13.6
	$0.32^{+0.03}_{-0.04}$		$1.98^{+0.15}_{-0.13}{}^b$	1.03/174	10.4
X9	$0.93^{+0.91}_{-0.72}$	$1.84^{+0.56}_{-0.38}$		0.5/3	1.45
X12	$0.16^{+0.28}_{-0.13}$		$0.17^{+0.06}_{-0.05}$	1.48/10	0.29
X13	$2.94^{+0.48}_{-0.43}$	$2.16^{+0.23}_{-0.21}$		1.25/47	25.1
	$1.81^{+0.29}_{-0.25}$		$2.00^{+0.24}_{-0.21}{}^b$	1.02/47	13.9
X19	$0.61^{+0.47}_{-0.46}$	$1.75^{+0.33}_{-1.18}$		1.02/4	1.24
X20	$0.62^{+0.35}_{-0.34}$		$0.10^{+0.04}_{-0.03}$	1.1/6	3.18
X21	$0.32^{+0.05}_{-0.05}$	$2.53^{+0.16}_{-0.16}$		1.50/82	3.88
	$0.08^{+0.02}_{-0.02}$		$0.86^{+0.04}_{-0.04}{}^b$	2.04/82	2.19
	$0.87^{+0.13}_{-0.25}$	$2.73^{+0.08}_{-0.16}$	$0.11^{+0.02}_{-0.02}{}^b$	1.25/80	29.3
	$0.75^{+0.34}_{-0.18}$	$1.66^{+0.12}_{-0.22}$	$0.10^{+0.02}_{-0.02}{}^c$	1.24/80	17.5
X26	$0.60^{+0.33}_{-0.27}$	$2.11^{+0.42}_{-0.37}$		0.77/14	3.49
X30	$0.51^{+0.33}_{-0.11}$	$2.85^{+0.97}_{-0.61}$		0.97/8	0.79
X31	$0.57^{+0.24}_{-0.27}$	$3.22^{+1.02}_{-0.64}$		0.54/8	0.93
X33	$0.67^{+0.62}_{-0.30}$	$2.42^{+0.96}_{-0.53}$		0.77/7	0.97

All quoted uncertainties are at the 90% confidence level.
^{a} Unabsorbed luminosity ($\times 10^{38}$ erg s^{-1}) in 0.5-10 keV, assuming a distance of 1.8 Mpc.
^{b} Disc blackbody temperature.
^{c} Blackbody temperature from the BMC model.

about 3 background sources accroding to the *Chandra* Deep Field Surveys (e.g., Brandt et al. 2001; Giacconi et al. 2001).

4 DISCUSSION

4.1 Global properties

Of the 37 detected X-ray sources in the field iof IC 342, 25 of them are inside the D_{25} ellipse. Based on the colour-colour diagram and spectral fits, X-ray sources in IC 342 are likely to be typical X-ray binaries. There are four sources for which the colours are similar to supernova remnants (see e.g., So-
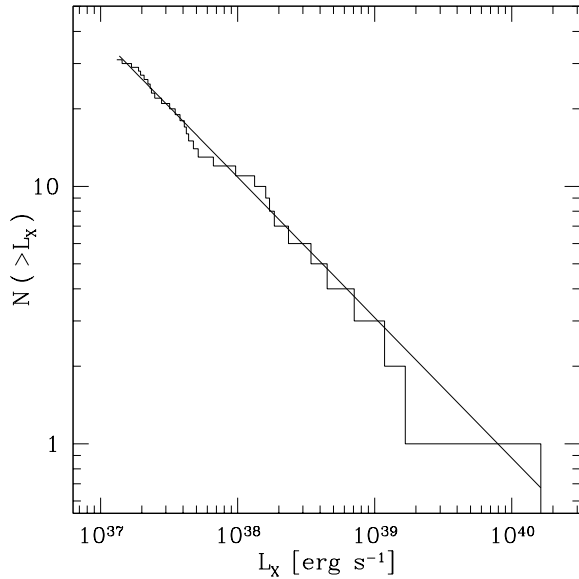
Figure 7. Cumulative luminosity function of X-ray point sources in IC 342. The best-fitting model is a power-law with slope $\Gamma = 0.55$.

ria & Kong 2003), while X20 is likely to be a luminous supersoft X-ray source (SSS; Di Stefano & Kong 2003). In a detailed study of SSSs in 4 external galaxies, Di Stefano & Kong (2003) found more than 30 SSSs while only one SSS in M101 has luminosity $> 10^{39}$ erg s^{-1} (see also Mukai et al. 2003). Recently, Kong & Di Stefano (2003) also discovered a recurrent luminous SSS in NGC 300 which exceeds 10^{39} erg s^{-1} during its high state. Therefore, X20 is one of the few very luminous SSSs found in nearby galaxies. Like many SSSs in external galaxies, it is clear that X20 is on the spiral arm of IC 342 (see Figure 3) where young stellar populations are expected. Comparing the fluxes between the *ROSAT* and *XMM-Newton* observations, X20 varies by a factor of 2, suggesting that it is unlikely to be a supernova remnant. It is therefore possible that X20 is a symbiotic if the accreting object is a white dwarf. However, in order to achieve such a high luminosity, it is likely that X20 contains a black hole accretor (see Di Stefano & Kong 2003 and Kong & Di Stefano 2003 for discussion). The spectral parameters ($kT = 100$ eV, $L_{bol} = 1.1 \times 10^{39}$ erg s^{-1}) is consistent with a model of an intermediate mass black hole (Di Stefano et al. 2003). The implied black hole mass would be at least $1200 M_{\odot}$. This is likely to be a lower limit as spectral hardening, orientation and spin would tend to increase the black hole mass. An alternative model involves an Compton thick outflow from a stellar-mass black hole, accreting near the Eddington limit (King & Pounds 2003). For instance, a 100 eV source is consistent with a $10 M_{\odot}$ black hole with an outflow rate of $10 \dot{M}_{Edd}$.

The point source luminosity function of IC 342 can be fit with a power-law and the slope ($\Gamma = 0.55$) is consistent with other starburst galaxies or spiral disc ($\Gamma \sim 0.5 - 0.8$; Kilgard et al. 2002; Grimm, Gilfanov, & Sunyaev 2003). Moreover, Grimm, Gilfanov, & Sunyaev (2002) obtained a slope of 0.6 for the high-mass X-ray binaries (HMXBs) in our Galaxy. The similarity between the luminosity functions of IC 342, Galactic HMXBs, and other starburst galaxies suggests that the X-ray point source population might be dominated by HMXBs with continuous star forming activity. More recently, Ranalli, Comastri & Setti (2003) determined a linear relation between the star formation rate (SFR) and total X-ray luminosity (2–10 keV) in various nearby star-forming galaxies based on *ASCA* and *BeppoSAX* data. In our *XMM-Newton* observation, the 2–10 keV luminosity of all point sources is $\approx 2.5 \times 10^{39}$ erg s^{-1}. Applying the relationship derived by Ranalli et al. (2003), we obtained a SFR of $\approx 0.5 M_{\odot}$ yr^{-1}. This is consistent with the SFR ($0.48 M_{\odot}$ yr^{-1}) obtained from radio observations (Grimm, et al. 2003). However, for such a low SFR, the relation between the SFR and X-ray luminosity is non-linear (Grimm et al. 2003). Following Grimm et al. (2003), the expected SFR from the observed X-ray luminosity should be between $0.3 - 1 M_{\odot}$ yr^{-1}.

4.2   X-ray emission from the nucleus

Although it was known that there is X-ray emission from the nucleus of IC 342 since *Einstein*, we know very little about its nature. *ROSAT* HRI image resolved the nucleus into several X-ray sources, but subsequent *ASCA* observations do not have the resolving power to isolate them. Furthermore, the *ROSAT* HRI image indicates that the nuclear source is extended. In the *XMM-Newton* observation, X21 is clearly seen and separated from nearby sources in the *XMM-Newton* image (see Figure 1) and is about 3″ from the dynamical galaxy centre. We examined the surface brightness profile of the source and it is consistent with the instrumental point spread function of a point source. Given a relatively large error circle ($\sim 4''$) from *XMM-Newton* data, it is not clear if X21 is truly associated with the dynamical centre. Better astrometry by *Chandra* is needed to confirm the result. From optical and infrared observations, there is a star cluster in the centre of the galaxy (Böker, van der Marel, & Vacca 1999). While a central black hole is not found, an upper limit of $5 \times 10^5 M_{\odot}$ can be set. We obtained the X-ray spectrum of X21. The source is very luminous ($\sim 10^{40}$ erg s^{-1} in 0.2–12 keV) and it requires two-component models to give a best fit. The result is similar to many ULXs in external galaxies and Galactic black hole binaries during the high/soft state. However, the disc temperature ($kT \approx 0.1$ keV) is about 5 to 10 times lower than expected. Recently, such cool disc systems have been found in NGC 1313 and have been interpreted as evidence of intermediate-mass black holes (Miller et al. 2003). Following Miller et al. (2003), the black hole mass of X21 is in the range of $220 M_{\odot}$ and $15000 M_{\odot}$. If we simply scale the mass according to the Eddington luminosity, we obtain a minimum black hole mass of $120 M_{\odot}$. However, the powerlaw component of X21 is weak and contributes only $\sim 10\%$ of the total emission. For the two ULXs in NGC 1313, the powerlaw compontent is 33% and 63% of the total X-ray flux (Miller te al. 2003). The unphysical spectral fit with broken powerlaw model rules out the possibility of an accreting stellar black hole with beamed relativistic jet emission (Kaaret et al. 2003). If X21 is indeed an intermediate-mass black hole, it is likely that the source is associated with the star cluster instead of the galaxy dynamical centre. Ebisuzaki et al. (2001) recently suggest that intermediate-mass black holes can form in young compact

star clusters through successive mergings of massive stars. This is suggestive that X21 is an example of this scenario. It is, however, worth to noting that we cannot rule out a stellar-mass black hole with strong wind (King & Pounds 2003; see also §4.1).

4.3 The ultraluminous sources in IC 342

Except for the nucleus, there are two historical ULXs (X7 and X13) in IC 342. We examined the light curves of the individual ULXs and they do not show significant variability on the timescale of our observation. The brightest off-nucleus ULX, X7, has a luminosity of $\sim 10^{39} \, \mathrm{erg \, s^{-1}}$ during the *XMM-Newton* observation. Comparing to previous *ASCA* observations, the source is consistent with the low/hard state (Kubota et al. 2001; see also Kubota, Done & Makishima 2002). Similarly, the luminosity state of the second brightest ULX, X13, during our *XMM-Newton* observation also corresponds to the low/hard state in the *ASCA* observations. It is worth noting that all previous X-ray observations derived the luminosity by assuming a distance of 4 Mpc which is greater than generally acceptable value of 1.8 Mpc (Buta and McCall 1999). We here rescaled all the luminosities assuming 1.8 Mpc. The smaller implied luminosities of the two brightest ULXs are still between $\sim 10^{39} - 10^{40} \, \mathrm{erg \, s^{-1}}$. Hence, a smaller black hole mass is required. For instance, according to the calculation by Kubota et al. (2002), X7 would have a black hole mass between $10 M_\odot$ and $30 M_\odot$.

It is clear from the *XMM-Newton* and *ROSAT* (Bregman et al. 1993) images that the two ULXs with state/intensity changes have several nearby sources. The significant poorer spatial resolution of *ASCA* (FWHM $> 1'$) and the large extraction radius ($3'$) used in analysing the *ASCA* data (Okada et al. 1998) imply that the targets suffer confusion problem. For example, a $3'$ circular region surrounding X7 includes six other sources (X6, X9, X12, X14, X15, and X16). Comparing the *XMM-Newton* counts of these sources, about 40% of the *ASCA* counts of X7 in the low state are due to confusion. Therefore, the luminosities measured by *ASCA* are over-estimated particularly during the low luminosity state. In fact, the two ULXs shown in Figure 1 in Kubota et al. (2001) show asymmetric shape and the centroids have moved during the two observations, indicating that there are bright nearby X-ray variables. Comparing the *XMM-Newton* data with the *ROSAT* HRI observations, X6 and X9 (not detected in Bregman et al. 1993, but might be marginally seen in the archival image) varied by a factor of > 2. It is therefore possible that the factor of ~ 5 (after correcting the possible confusion of nearby sources based on *XMM-Newton* data) variability of X7 during the two *ASCA* observations are due to X6 and X9, and/or other nearby sources if one of these sources varies by at least a factor of 10. It is more likely that the variability seen by *ASCA* is intrinsic to X7. In addition, X12 is a foreground star which shows soft spectrum (see Table 2). If the foreground star has flarings during the high/soft state in the *ASCA* observations, it could contribute additional soft X-ray emission.

More recently, X7 was observed by *Chandra* ACIS-S on 2002 April 29 with an exposure time of 10 ks. We therefore use this archival observation to investigate the contamination of nearby sources in detail. Within $30''$ of X7, there is no

obvious X-ray source and the nearest point source is about $3.6'$ from X7 [1]. Any faint source within this area must be fainter than $8 \times 10^{36} \, \mathrm{erg \, s^{-1}}$. Hence, the contamination of our *XMM-Newton* spectrum should be minimal. We also examined the *Chandra* spectrum of X7. After correcting the soft energy degradation and pile-up ($\sim 5\%$), the spectrum can be fit with a power-law model [$N_H = (5.68 \pm 0.09) \times 10^{21} \, \mathrm{cm^{-2}}$, $\alpha = 1.81 \pm 0.31$] with a reduced χ^2 of 1.0 for 81 degrees of freedom. The 0.5–10 keV luminosity is $1.6 \times 10^{39} \, \mathrm{erg \, s^{-1}}$, similar to our *XMM-Newton* observation.

Similarly, for X13, a $3'$ extraction region covers X11 and X20 as well. In particular, X20 is likely to be a luminous ($\sim 10^{39} \, \mathrm{erg \, s^{-1}}$ in 0.5–10 keV) SSS (see Table 2 and §4.1 for discussion) and it shows a factor of 2 variability between the *ROSAT* and *XMM-Newton* observations. SSSs are well-known to be highly variables (e.g., Di Stefano & Kong 2003; Kong & Di Stefano 2003) and therefore the less than factor of 2 variability of X13 during the two *ASCA* observaitons is easily explained by the existence of a SSS. Note that the SSS has relatively high temperature ($kT = 0.1$ keV) and *ASCA* should be able to detect it; the source luminosity in the *ASCA* band (0.7–10 keV) is about $9 \times 10^{37} \, \mathrm{erg \, s^{-1}}$. Comparing with the 0.7–2 keV *ASCA* count rate of X13 during the high state (Sugiho et al. 2001), roughly 25% of counts are contaminated by the SSS (assuming the same blackbody model measured by *XMM-Newton*). Therefore, if the SSS brightens during the high state by a factor of > 2, it could contribute significant soft photons to result a softer and brighter spectrum. It is worth noting that X13 is asymmetric toward the direction of the supersoft source, X20, during the high/soft state in 2000 (see Figure 1 in Kubota et al. 2001). We therefore conclude that the spectral/intensity changes seen in the two *ASCA* observations should be treated with caution. Further monitoring observations with *XMM-Newton* and *Chandra* are required to investigate the state transitions of ULXs in IC 342.

5 SUMMARY

We have studied the X-ray point source population in the nearby starburst galaxy IC 342 with *XMM-Newton*. Thirty-seven X-ray sources were detected at a significance of 5σ or greater. The X-ray point source luminosity function is in a power-law form and the slope ($\Gamma = 0.55$) is consistent with other starburst galaxies and Galactic HMXBs. Most of the X-ray sources are near the spiral arms, indicating that the X-ray point sources are dominated by young stellar population (presumably HMXBs) with continuous star forming activity. For the 12 brightest sources, we extracted the energy spectra and except for the nucleus, a SSS, and a foreground star, they can be described by a power-law model. There is one source (X21) about $3''$ from the dynamical centre, and the spectrum can be fit with a disc blackbody plus power-law model. The source is very luminous ($\sim 10^{40} \, \mathrm{erg \, s^{-1}}$) and the disc temperature is low ($kT = 0.11$ keV). It could be

---

[1] The *Chandra* observation was operated in sub-array mode and therefore it only covered a small part around X7. From our *XMM-Newton* observation, the nearest point source to X7 is about $50''$ away.

an evidence for an intermediate-mass black hole or a stellar-mass black hole with strong wind. We also investigate the intensity/spectral changes of the two famous ULXs but our *XMM-Newton* observation suggests that the changes could be simply due to confusion of *ASCA* observations.

REFERENCES

Becklin, E.E., Gatley, I., Matthrews, K., Neugebauer, G., Sellgren, K., Werner, M.W., Wynn-Williams, C.G., 1980, ApJ, 236, 441

Böker, T., van der Marel, R., & Vacca, W.D., 1999, AJ, 118, 831

Brandt, W.N. et al. 2001, AJ, 122, 2810

Bregman, J.N., Cox, C., Tomisakam K., 1993, ApJ, 415, L79

Buta, R.J., McCall, M.L., 1999, ApJS, 124, 33

Crawford, D.F., Jauncey, D.L., Murdoch, H.S., 1970, ApJ, 162, 405

Dickey, J.M., Lockman, F.J., 1990, ARA&A, 28, 215

Di Stefano, R., Kong, A.K.H., 2003, ApJ, 592, 884

Di Stefano, R., Kong, A.K.H., Greiner, J., Primini, F.A., Garcia, M.R., Barmby, P., Massey, P., Hodge, P.W., Williams, B.F., Murray, S.S., Curry, S., Russo, T.A., 2003, ApJ, submitted (astro-ph/0306440)

Ebisuzaki, T., et al., 2001, ApJ, 562, L19

Fabbiano, G., Trinchieri, G., 1987, ApJ, 315, 46

Giacconi, R. et al. 2001, ApJ, 551, 624

Grimm, H.-J., Gilfanov, M., Sunyaev, R., 2002, A&A, 391, 923

Grimm, H.-J., Gilfanov, M., Sunyaev, R., 2003, MNRAS, 339, 793

Kaaret, P., Corbel, S., Prestwich, A.H., Zezas, A., 2003, Science, 299, 365

Kilgard, R.E., Kaaret, P., Krauss, M.I., Pretwich, A.H., Raley, M.T., Zezas, A., 2002, ApJ, 573, 138

King, A.R., Pounds, K.A., 2003, MNRAS, in press (astro-ph/0305541)

Kong, A.K.H., Garcia, M.R., Primini, F.A., Murray, S.S., Di Stefano, R., McClintock, J.E., 2002, ApJ, 577, 738

Kong, A.K.H., Di Stefano, R., 2003, ApJ, 590, L13

Kubota, A., Mizuno, T., Makishima, K., Fukazawa, Y., Kotoku, J., Ohnishi, T., Tashiro, M., 2001, ApJ, 547, L119

Kubota, A., Done, C., Makishima, K., 2002, MNRAS, 337, L11

Miller, J.M., Fabbiano, G., Miller, M.C., Fabian, A.C., 2003, ApJ, 585, L37

Monet, D., et al., 1998, The USNO-A2.0 Catalogue (Flagstaff: US Naval Obs.)

Mukai, K., Pence, W.D., Snowden, S. L., Kuntz, K.D., 2003, ApJ, 582, 184

Newton, K., 1980, MNRAS, 191, 169

Okada, K., Dotani, T., Makishima, K., Mitsuda, K., Mihara, T., 1998, PASJ, 50, 25

Ranalli, P., Comastri, A., Setti, G., 2003, A&A, 399, 39

Rickard, L.J., Harvey, P.M., 1984, AJ, 89, 1520

Roberts, T.P., Warwick, R.S., 2000, MNRAS, 315, 98

Shrader, C.R., Titarchuk, L., 1999, ApJ, 521, L121

Soria, R., Kong, A.K.H., 2003, A&A, submitted

Sugiho, M., Kotoku, J., Makishima, K., Kubota, A., Mizuno, T., Fukazawa, Y., Tashiro, M., 2001, ApJ, 561, L73

Turner, J.L., Hurt, R.L., 1992, ApJ, 384, 72

Wu, K., 2001, PASA, 18, 443